ACSNANO

www.acsnano.org Article

Ferromagnetic Ordering in Rashba Superconductive $LaAl_{0.7}Mn_{0.3}O_3$/$SrTiO_3$ Interface

Yulin Gan,* Yuhao Hong, Guang Yang, Qinghua Zhang, Wen Xiao, Lei Wang, Shilin Hu, Jie Shen, Lei Yan, Li Lu, Philippe Ohresser, Kai Chen,* Hong Ding,* and Zhaoliang Liao*

Cite This: *ACS Nano* 2026, 20, 4343−4351

Read Online

ACCESS | Metrics & More | Article Recommendations | Supporting Information

ABSTRACT: The combination of ferromagnetism, superconductivity, and spin−orbit coupling in interfacial two-dimensional electron liquids (2DELs) assembles the essential ingredients for realizing tantalized topological or spin polarized superconductivity for interfacial oxitronics. Unfortunately, these ingredients usually compete and are sometimes mutually exclusive. Here, by optimally designing a ferromagnet/superconductor heterostructure ($LaAl_{0.7}Mn_{0.3}O_3$/$SrTiO_3$), we demonstrate a ferromagnetic 2DEL with strong Rashba spin−orbit coupling and typical superconducting behavior. More excitingly, Rashba spin−orbit coupling and ferromagnetic order were found to coexist according to the observation of weak antilocalization and butterfly shaped magnetoresistance with clear hysteresis during the superconducting transition. Our revealed coexistence of ferromagnetism, superconductivity, and spin−orbit coupling at the oxide interface provides a fruitful platform to investigate nontrivial properties of spin-polarized supercurrent/topological superconductors and to cultivate applications for superconducting spintronics/quantum computation.

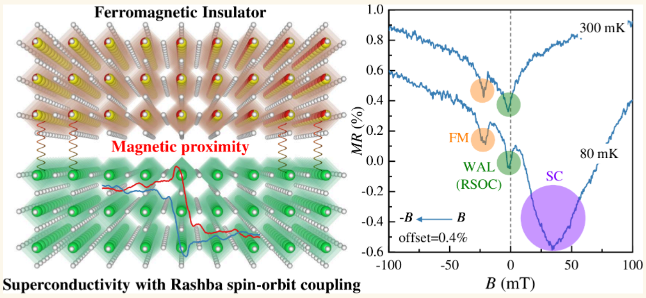

KEYWORDS: *ferromagnet/superconductor heterostructure, ferromagnetism, Rashba spin−orbit coupling, superconductivity, magneto transport*

To realize the entanglement between superconductivity (SC), ferromagnetism (FM), and further spin−orbit coupling (SOC) is a highly pursued goal owing to their extraordinary physical properties, such as spin-polarized supercurrent for superconducting spintronics,[1] spin−orbitronics,[2] and magnetic vortex/Fulde−Ferrell−Larkin−Ovchinnikov state in topological superconductors for quantum computation.[3−6] However, superconductivity and ferromagnetism are usually competing, and materials with coexistence of superconductivity and ferromagnetism are very rare. Furthermore, materials with large SOC usually are hosted by heavy elements, which favor delocalized and extended orbitals, thus not favoring ferromagnetism. Therefore, many ferromagnetic materials usually exhibit small SOC. As a result, it is extremely challenging to synthesize a material system where all these intriguing ingredients can coexist. Benefiting from state-of-the-art deposition technology, atomic scale growth of heterostructures is now feasible where different types of materials can now be artificially integrated and combined, thus generating functional interfaces for realization of emergent physical phenomena beyond their bulk counterparts. For example, an artificially grown ferromagnet/superconductor heterostructure with interfacial Rashba SOC (RSOC) as shown in Figure 1a[4,7] can effectively lead to fantastic ferromagnetic coupled Rashba superconductivity for low-power logic devices,[8−10] especially the magnetization-controlled nonreciprocal transport near or inside the superconducting states.

The strongly correlated two-dimensional liquid (2DEL) at $SrTiO_3$ (STO) or $KTaO_3$ (KTO) based heterointerfaces is a very promising candidate to explore these nontrivial states of matter with coexistence of SC, FM, and SOC, due to its highly tunable SC,[11−15] FM,[16−21] and RSOC.[22−26] At the paradigmatic interface between $LaAlO_3$ (LAO) and STO or KTO, strong RSOC and SC have been found,[12,22,25,27] boosting the research of 2D Rashba SC at oxide heterostructures.[24,28,29] Furthermore, hybridizing such heterostructures with magnetic elements is an effective and powerful method to introduce magnetism into 2DEL through magnetic proximity effect,[18,30−32] despite nonmagnetic insulating STO and KTO. Though these properties have been extensively investigated, current research mainly separately investigates their behaviors. For example, most cases studied the FM from the anomalous Hall effect (AHE) and SOC from the weak antilocalization

Received: October 16, 2025
Revised: January 14, 2026
Accepted: January 15, 2026
Published: January 28, 2026

https://doi.org/10.1021/acsnano.5c17832

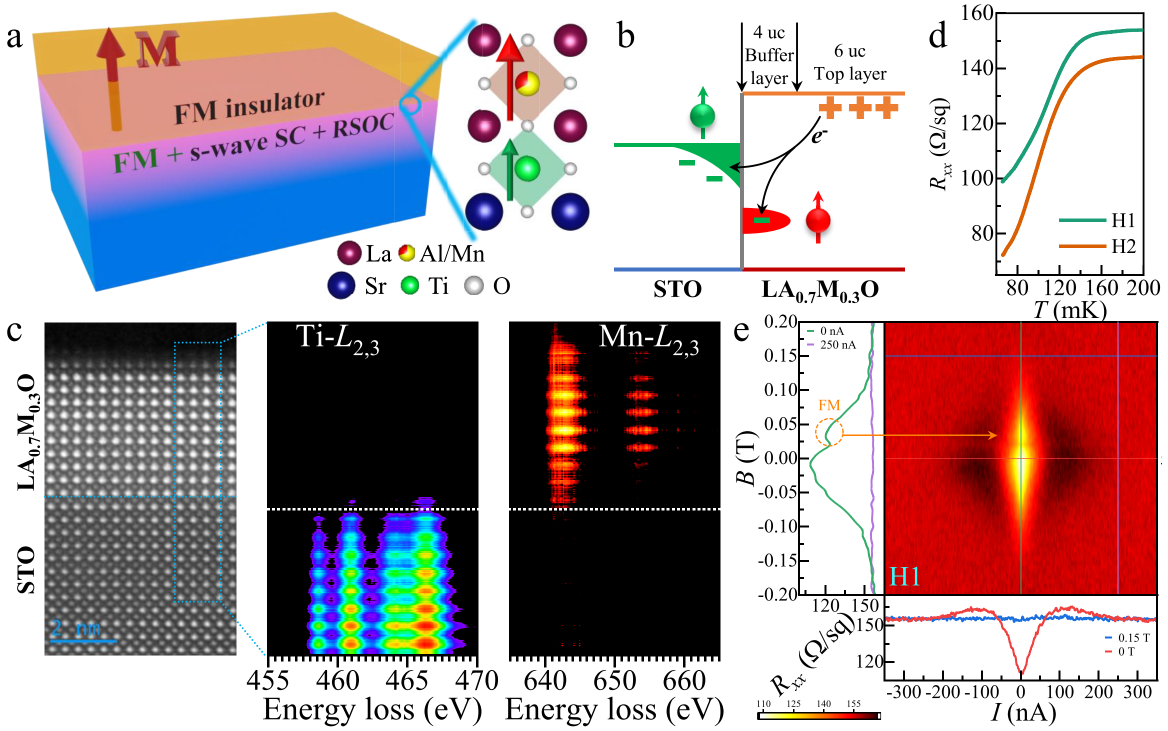

Figure 1. Fabrication of oxide ferromagnet/superconductor heterointerfaces. (a) A sketch of oxide ferromagnet/superconductor heterointerfaces with the 2DEL, which is designed to combine the FM, SC, and RSOC. (b) Schematic band diagram of such $LA_{0.7}M_{0.3}O$/STO. Given the alignment of O 2p bands at such heterointerface, the empty e_g^2 band of LAMO with lower energy than Ti 3d t_{2g} bands provides an electron sink to modulate the interface. The electrons from top layer first occupy the Mn sites and then transfer into the conduction band of Ti at the interface. (c) The HAADF-STEM images, spatially resolved Ti $L_{2,3}$ and Mn $L_{2,3}$ EELS spectra about the heterointerface. (d) The sheet resistance as a function of temperature down to 70 mK for two heterostructures. (e) The R_{xx} at 70 mK as a function of I_{bias} and B, where the I_{bias} scans from −350 to 350 nA and B is increased from −0.2 to 0.2 T. The lower panel shows the horizontal line cuts at B = 0 T (red) and 0.15 T (blue), and the left panel shows the vertical line cuts at I_{bias} = 0 nA (green) and 250 nA (violet).

(WAL) effect in normal state. Although the coexistence between any two of the three phenomena—SC, FM, and SOC—has been experimentally established,[24,33−37] comprehensive investigations into their tripartite interplay has been notably absent. How FM and SOC behave at the SC state and how to probe their possibility of coexistence remain open problems.

In this work, we rationally designed a $LaAl_{1-x}Mn_xO_3$/$SrTiO_3$ (LAMO/STO, $0 \le x \le 1$) heterointerfaces with proper doping level x and carrier density in order to realize coexistence of FM, SC, and RSOC. The introduction of an insulating LAMO thin film can reduce carrier density, and at the same time it can exhibit strong magnetism with high Mn doping level. Therefore, the interfacial carrier density (n_s), AHE induced by the magnetic proximity effect, and SC can be tuned by changing Mn doping level. Previous reports[32,38] have shown the possible coexistence of FM and RSOC for interfaces with x = 0.25 or 0.3. Therefore, $LaAl_{0.7}Mn_{0.3}O_3$ is optimal doping level to generate magnetism and at the same time to induce superconducting 2DEL at the LAMO/STO interface, where both AHE and SC are observed at 7.6×10^{12} cm^{-2} < n_s < 1.3×10^{13} cm^{-2}.[32] With these, we intentionally fabricate two $LA_{0.7}M_{0.3}O$/STO samples with n_s of 9.74×10^{12} cm^{-2} (heterostructure 1: H1) and 1.13×10^{13} cm^{-2} (heterostructure 2: H2) located in the coexistence regime between FM and SC by precisely controlling the growth conditions. The investigations of hysteretic butterfly magnetoresistance (MR), the hysteretic anomalous Hall effect (HAHE), and X-ray magnetic circular dichroism (XMCD) confirm the FM of 2DELs. Meanwhile, the WAL reveals the RSOC of such 2DEL. Most importantly, both the FM-induced butterfly hysteresis and RSOC-induced WAL have been observed in MR during the superconducting transition, demonstrating the coexistence of FM, RSOC, and SC directly. Additionally, the 2DEL contributed by Ti t_{2g} electrons was found to have a 2D d_{xy} feature. Our results provide conclusive evidence of an emergent Rashba-type superconductivity interwoven with ferromagnetic ordering at the $LA_{0.7}M_{0.3}O$/STO interface.

RESULTS AND DISCUSSION

Optimized $LA_{0.7}M_{0.3}O$/STO heterointerfaces with carrier density at coexistence regimes of FM and SC[32] were prepared by growing a 4 unit cell (uc) buffer layer at 1×10^{-4} mbar of O_2 at first and then depositing the 6 uc top layer at 1×10^{-5} mbar of O_2. A schematic band diagram in Figure 1b illustrates the formation of ferromagnetic 2DELs at the oxide ferromagnet/superconductor heterointerfaces. For the magnetism, the buffer layer grown at higher pressure can result in stronger ferromagnetism of $LA_{0.7}M_{0.3}O$[39] and thus can induce stronger magnetism of 2DELs by the proximity effect.[32] Meanwhile, the introduction of $LaMnO_3$ into $LaAlO_3$/$SrTiO_3$ heterostructures not only provides an electron sink to trap the electrons at interfaces[40] and but also reduces the oxygen outward diffusion effectively.[41] For the 10 uc $LA_{0.7}M_{0.3}O$ film grown at 1×10^{-4} mbar O_2 pressure, the insulating interface at low temperature confirms the negligible oxygen vacancy (Figure S2). Therefore, the interfacial oxygen vacancy can be reduced significantly, and the interfacial itinerant electrons of

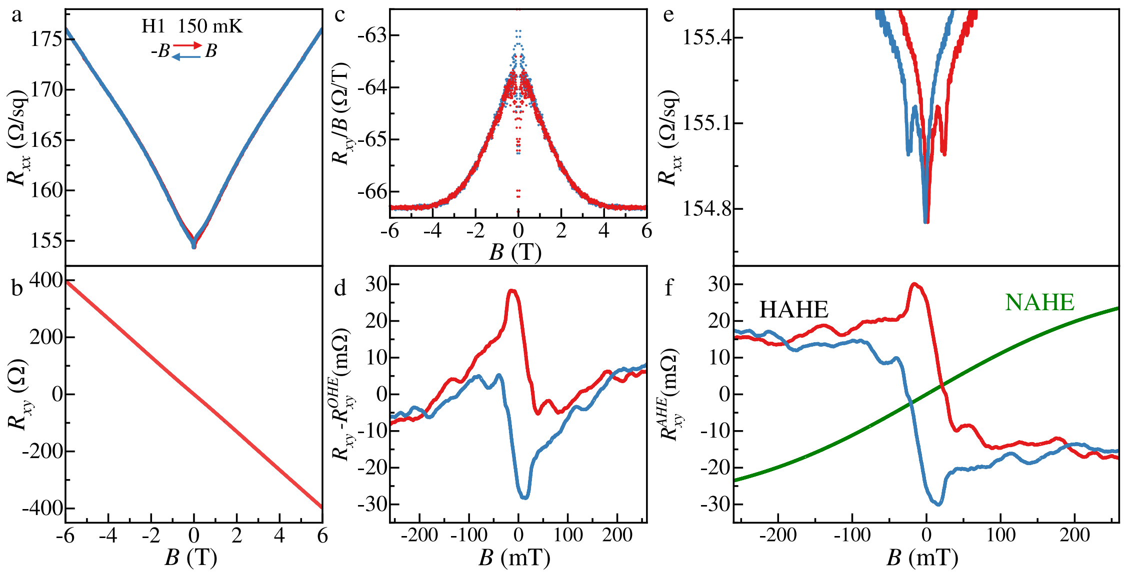

Figure 2. Analysis of magnetoresistance and Hall resistance of H1 at 150 mK. (a) The MR of H1 with the weak antilocalization around 0 T. (b) The Hall resistance of H1. (c) The R_{xy}/B shows an upturn at low fields up to ∼4 T and becomes a constant after 4 T, suggesting that the Hall resistance undergoes a transition from a nonlinear behavior to the linear behavior around 4 T. (d) A significant hysteretic loop below ∼30 mT superposed on a nonlinear Hall resistance without loop is observed when subtracting the linear ordinary Hall resistance. (e) A significant hysteretic butterfly MR superimposed on the weak antilocalization regime. (f) The total AHE in (d) includes the hysteretic anomalous Hall effect (HAHE) and the nonhysteretic anomalous Hall effect (NAHE).

2DELs arise from the top layer. The typical high-angle annular dark-field (HAADF) scanning transmission electron microscopy (STEM) image for such ferromagnet/superconductor heterostructure in Figure 1c reveals the chemically abrupt interface without detectable defects and dislocations. The spatially resolved Ti $L_{2,3}$ and Mn $L_{2,3}$ electron energy-loss spectroscopy (EELS) indicates the chemically abrupt heterointerface, where Mn ions are confined almost exclusively within the LAMO layer with negligible downward diffusion into the STO substrate and the Ti ion outward diffusion is less than one unit cell across the interface.

As shown in Figure 1d, temperature-dependent sheet resistance (R_{xx}) shows typical superconducting behavior at LA$_{0.7}$M$_{0.3}$O/STO interfaces, where the significant change of the corresponding slope (dR_{xx}/dT) indicates that the onset point of the superconducting transition is around 150 mK for both heterostructures (H1 and H2 in Figure S3). The superconductivity has been widely observed in the electron-doped STO such as the oxygen-deficient STO[15] and La-/Nb-/Sm-doped STO.[42] In our case, the carriers contributing such interfacial superconductivity stem from the LAMO top layer due to the negligible oxygen deficiencies at the STO side. Although the zero resistance was not detected down to the base temperature of our systems due to the lower superconducting transition temperature, the superconductivity has been confirmed in previous work.[32] Meanwhile, the differential resistance R_{xx} (dV/dI) of the 2DEL as a function of the bias current (I_{bias}) and the magnetic field (B) at 70 mK in Figure 1e provides an alternative method to further characterize the formation of interfacial superconductivity. For $B = 0$ T (the lower panel in Figure 1e), the sharp peaks at the critical current $I_c \approx 128$ nA and the dip in zero-bias R_{xx} suggest the highly nonlinear behavior of $V-I$ curves. With the increasing B, such nonlinear behavior is gradually suppressed, resulting in the transition from nonlinear behavior to ohmic behavior at the superconducting upper critical field (B_{c2}).[43] In addition, the U-shaped MR is observed clearly below the I_c, where B breaks the Cooper pairs and phase coherence with the B_{c2} of ∼120 mT (the left panel in the Figure 1e). The significant superconducting transition, the highly nonlinear $V-I$ behavior, and the U-shaped MR confirm the formation of Cooper pairs and the phase coherence within the 2DELs at LA$_{0.7}$M$_{0.3}$O/STO interfaces. Notably, a dip appears around 30 mT in the typical U-shaped superconducting regime[43] when sweeping the B from negative to positive (the left panel in the Figure 1e), which is similar to the ferromagnetism induced hysteretic butterfly MR,[44] which implies the coexistence of ferromagnetic order and superconductivity.

The further MR ($R_{xx}(B)/R_{xx}(0)$-1) characterization of H1 at 150 mK in Figure 2a shows a sharp dip at low field superposed on a quadratic MR background. Such a quadratic background arises from the ordinary MR caused by the classical Lorentz force. Moreover, the sharp dip around zero field indicates the presence of RSOC-induced WAL.[22,38] Strong RSOC caused by the absence of spatial inversion symmetry at heterointerfaces will break the quantum interference from electron phase coherence in weak localization, leading to WAL effect and thus a dip around zero field in MR curve.[38] A quantitative analysis based on the Maekawa−Fukuyama developed WAL theory[22,28,45] extracts the spin−orbit coupling field B_{so} of 0.025 T and the Rashba coefficient α_{so} $\left(\frac{\sqrt{e\hbar^3 B_{so}}}{m^*}\right)$ of ∼4.68 meVÅ for H1 in Figure S4. Meanwhile, according to the analysis of Hall resistance in previous investigations,[32,46] the Hall coefficient (R_{xy}/B in Figure 2c) from the Hall resistance in Figure 2b shows an upturn at low fields up to about 4 T and becomes a constant after 4 T, suggesting that the Hall resistance undergoes a transition from a nonlinear behavior at low field to the linear behavior at high field in Figure 2b. This is the typical AHE with one type of carrier.[19,21,32,38,46] Due to the lower energy of the d_{xy} band compared to the $d_{xz/yz}$ band within the t_{2g} conduction manifold of STO(001) inter-

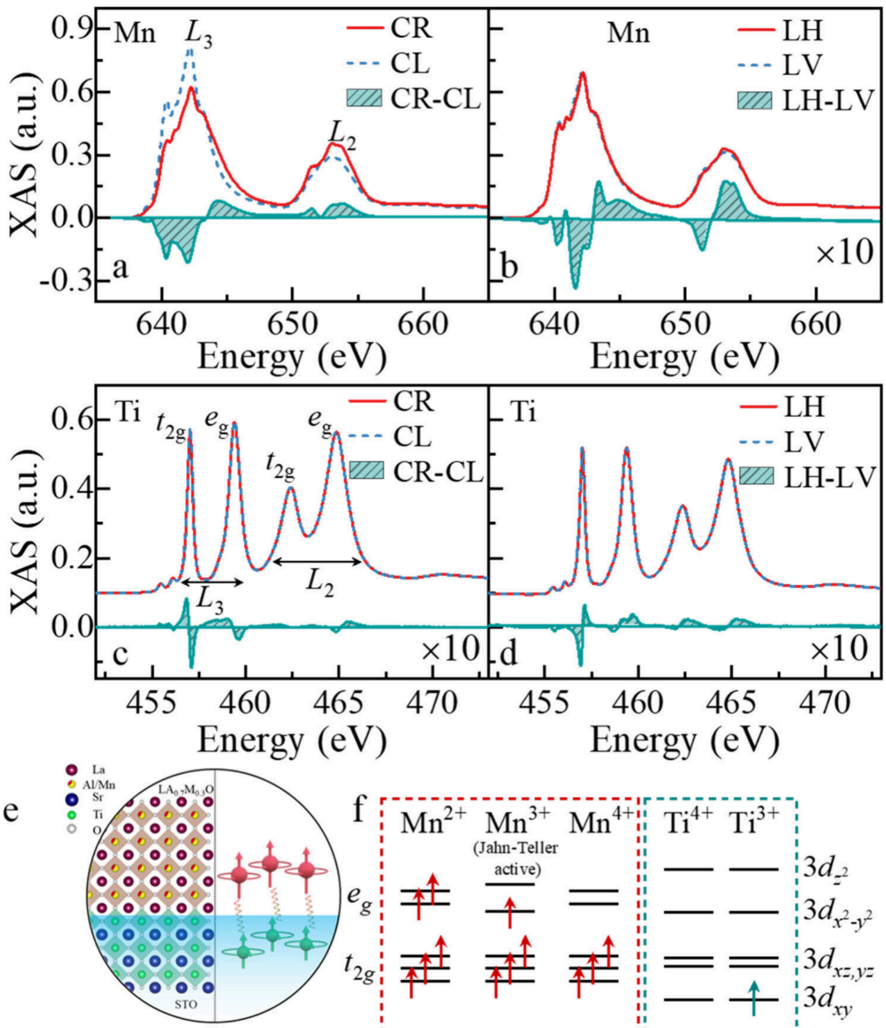

Figure 3. Origin of ferromagnetism. (a and c) XAS/XMCD spectra at Mn $L_{2,3}$ and Ti $L_{2,3}$ edges for normal incident sample orientation (90°). (b and d) XAS/XLD spectra of Mn and Ti for grazing (35°). All signals are collected under 6.5 T and 4 K. (e) A sketch of ferromagnetic coupling at the interface. (f) The orbital ordering and the spin states of the Mn and Ti.

face,[32,47−49] such 2DEL is primarily composed of the d_{xy} electrons. Interestingly, a hysteretic butterfly pattern is observed in the WAL regime when sweeping B in two opposite directions in Figure 2e, where this significant magnetic hysteresis is also manifested in the Hall resistance within the same low-field regime (see zoomed-in image in Figure S5). Notably, this Hall resistance hysteresis occurs below ∼30 mT in Figure S5, which is far lower than the broader nonlinear Hall regime spanning from −4 to 4 T in Figure 2c. To extract the anomalous Hall components, we subtract the linear ordinary Hall effect (OHE) from the Hall resistance in Figure 2b. The resulting anomalous Hall resistance in Figure 2d reveals a clear hysteretic loop superposed on a nonhysteretic, nonlinear background, suggesting that the total AHE includes the nonhysteretic anomalous Hall effect (NAHE) and the hysteretic anomalous Hall effect (HAHE). This NAHE dictates the overall nonlinearity of the Hall resistance and can be described by the Langevin-type function[46] ($R_{xy}^{\mathrm{NAHE}} = R_0^{\mathrm{NAHE}} \tanh(B/B_c)$) with two free parameters, B_c and R_0^{NAHE}. After further removal of the fitted NAHE component (green curve in Figure 2f), the purely HAHE is revealed in Figure 2f. This HAHE corresponds directly to the hysteretic butterfly MR shown in Figure 2e. The NAHE is consistent with previous observations of spin-polarized 2DELs at STO-based interfaces.[18,30,46] On the other hand, the HAHE both shows a typical conventional AHE proportion to the spontaneous magnetization,[50] and includes a hump-like Hall component that has been observed in some magnetic oxide materials with spin−orbit coupling, such as $SrRuO_3$,[51] $SrIrO_3/LaCoO_3$ superlattices,[52] and the $LaTiO_3/EuTiO_3$ interface.[53] A plausible origin of this hump-like feature in the Hall data is the topological Hall effect, a possibility that merits deeper study. Our work clearly disentangles these distinct AHE components in a strongly correlated oxide 2DEL. The concurrent hysteretic MR and AHE are characteristic of ferromagnetic conductors and imply the emergence of ferromagnetic order among the d_{xy} electrons in our system.[17,18,44] Importantly, the WAL, hysteretic butterfly MR, and HAHE confirm the coexistence of RSOC and FM at such superconducting interfaces.

To further confirm the ferromagnetism of $LA_{0.7}M_{0.3}O/STO$ systems, element-specific X-ray absorption spectroscopy (XAS) and XMCD at the Mn and Ti $L_{2,3}$ absorption edges were performed to probe the magnetism of the LAMO and the itinerant magnetism of 2DEL. The peaks of Mn L_3 edge XAS spectra (Figure 3a) at ∼640, ∼642, and 643 eV suggest the

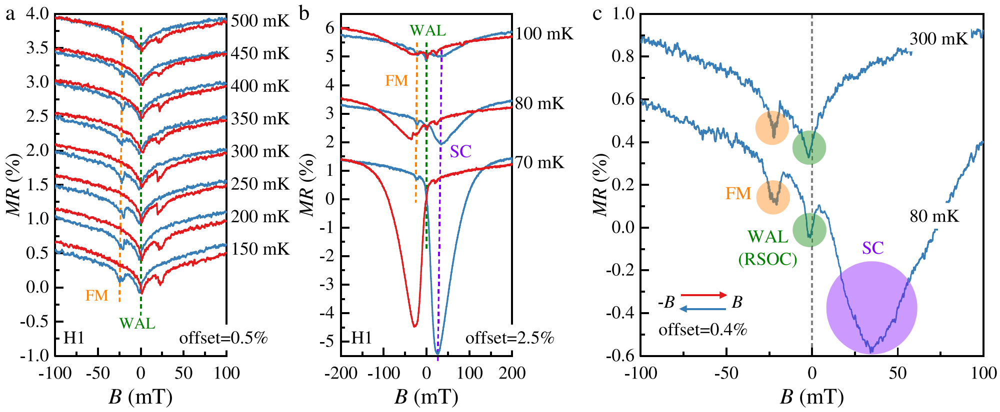

Figure 4. Coexistence of ferromagnetism, weak antilocalization, and superconductivity. The evolutions of MR upon cooling before (a) and after (b) the appearance of superconducting related MR (red and blue curves are from increasing and decreasing B, respectively). The typical features of FM, WAL, and SC are highlighted, respectively, taking decreasing B as an example (blue lines). (c) The typical behaviors of FM, WAL, and SC on the MR with decreasing B.

appearance of Mn^{2+}, Mn^{3+}, and Mn^{4+} states in LAMO, respectively (Figure S6).[54] The intensity of the Mn^{3+} peak indicates that the Mn^{3+} dominated in LAMO.[39] The appearance of Mn^{2+} could arise from the electron sink effect, where the electrons transfer first to Mn^{3+} empty e_g band with lower energy than the Ti^{4+} t_{2g} band before forming the interfacial 2DEL.[32] The significant XMCD signals at the Mn $L_{2,3}$ edges are observed around the peaks of Mn^{2+} and Mn^{3+}, ambiguously confirming the ferromagnetism of the $LA_{0.7}M_{0.3}O$ thin film. The X-ray linear dichroism (XLD) of Mn, defined as σ_{LH}-σ_{LV} (in Figure 3b), clearly reveals the degeneracy of e_g orbitals of the Jahn−Teller active Mn^{3+} ions. The positive integration of XLD (Figure S7b) indicates favorable in-plane $d_{x^2-y^2}$ occupation.

Owing to the magnetic proximity effect, the interfacial itinerant carriers would be spin-polarized by the ferromagnetic $LA_{0.7}M_{0.3}O$ thin film, resulting in ferromagnetic 2DELs and leading to the AHE in Figure 2. To confirm the magnetism of Ti at the interface, we further measured XMCD of Ti. As shown in Figure 3c, a clear XMCD signal is observed for Ti $L_{2,3}$ edges, thus definitely confirming the ferromagnetism of Ti at the interface. It is worth noting that the XAS of the Ti peak looks quite similar to the spectrum of Ti^{4+},[55] and thus suggests the dominating Ti^{4+} near the interface. However, since Ti^{4+} has nonmagnetic $3d^0$ configuration, the XMCD signal should be attributed to the small amount of spin-polarized Ti^{3+} state with $3d^1$ configuration.[55] The formation of 2DEL also suggests Ti^{3+} at the interface. Meanwhile, the XLD signal of the Ti L-edge shown in Figure 3d, with a profile similar to previous ones reported for LAO/STO heterostructures,[56] indicates the degeneracy of the Ti t_{2g} states. According to the very first negative feature near 457 eV and the resulting total positive integration (Figure S8), we conclude that the ferromagnetic itinerant carriers are mainly populated by d_{xy} of the t_{2g} orbitals. Such orbital degeneracy revealed by XLD is well consistent with the scenario speculated from the carrier density, as discussed above, which is below the Lifshitz transition and suggests the d_{xy} orbit of 2DEL.[32,57] The XMCD sum rule[58−60] was used to quantitatively estimate the magnetization of Mn and Ti (Figures S7a and S8a). Following Hund's rules, for the $3d^1$ configuration of Ti^{3+}, we obtain a positive Ti spin moment (0.013 μ_B) and an opposite, finite, negative Ti orbital moment (−0.012 μ_B). Importantly, the observed positive Mn-spin moment of 2.18 μ_B confirms that the Ti spin is ferromagnetically coupled to the Mn-spin moment. The ferromagnetic coupling between Mn^{3+} and Ti^{3+} sites in $La_{0.7}M_{0.3}O$/STO is different from the oxygen defects induced magnetism[55,61] and the antiferromagnetic coupling between Ti and Eu sites in the $LaAlO_3$/$EuTiO_3$/$SrTiO_3$ system.[30] All spectral results suggest the interfacial ferromagnetic coupling as shown in Figure 3e, where the ferromagnetism of Mn induces the spin-polarization of carriers at the Ti $3d_{xy}$ orbit, and the corresponding orbital orderings are shown in Figure 3f.

The R_{xx} of superconductivity under the I_{bias} in Figure 1e and the magneto transport characterization in Figure 2 imply the possible coexistence of RSOC, FM, and SC in the 2DEL at $LA_{0.7}M_{0.3}O$/STO interfaces. The MR curves around the superconducting transition are further analyzed in order to verify their coexistence and evolution. For $T \geq 150$ mK in Figure 4a, a dip around 23 mT is superposed on the WAL-induced background MR for a positive field sweep. When reversing the sweeping direction, the appearance of mirror dip gives rise to a hysteretic butterfly pattern. Such hysteretic butterfly behavior suggests the underlying ferromagnetic order in 2D itinerate carriers. These transport signatures in normal states indicate the coupling between FM and RSOC. When the temperature is lower than 150 mK (Figure 4b), an interesting parabolic dip emerges and results in a minimum around −30 mT, prior to appearance of WAL for positive field sweep. With cooling, the amplitude and width of the parabolic dip rapidly increase, which is the feature of superconductivity and is in agreement with the results in Figure 1e. These collective observations suggest that such a significant parabolic dip in the MR curve is from the superconducting fluctuation during the superconducting transition, where the Cooper pairs significantly enhance the overall conductivity. The similar MR behavior exhibited by both WAL and superconducting fluctuations[62−64] makes it difficult to deconvolve the superimposed signals, especially when the superconducting component dominates at low temperatures. Therefore, the superconducting fluctuation progressively coalesces with the WAL during cooling, leaving two dips at 70 mK. Much more interestingly, a mirror image of the superconducting and ferromagnetic dips is observed for a negative field sweep. Because the MR of superconducting states should be B-symmetric without the hysteresis for the typical oxide superconducting interfaces without FM,[43,65] the hysteretic superconducting MR in Figure 4b could be attributed to the FM-induced compression of SC around the ferromagnetic MR dips,[66] which has been widely observed in the FI/SC/FI (FI: ferromagnetic insulator) structures.[67] The direct observation of ferromagnetic ordering and RSOC at our oxide ferromagnet/superconductor heterointerfaces confirms the coexistence of out-of-plane FM, SC, and RSOC, which are the necessary ingredients to realize a designer topological superconductor.[4,7] Due to the RSOC induced the spin splitting of energy band structure and the spin-momentum locking, the combination of SC and RSOC stabilizes a Rashba-type pairing symmetry in superconductors,[68,69] and such heterointerfaces provide wonderful platforms to investigate the nonreciprocal transport by controllable magnetization near or inside the superconducting phase.[70] Furthermore, such oxide ferromagnet/superconductor heterointerfaces would have interesting implications for the controllable magnetic vortex in quantum computation.

CONCLUSIONS

In summary, we directly observed the combination of FM, SC, and RSOC in the 2DELs by rationally designing oxide ferromagnet/superconductor heterointerfaces ($LA_{0.7}M_{0.3}O$/STO) (Figure 4c). Our analysis unveils a hysteretic component in the anomalous Hall resistance. The presence of a conventional hysteretic anomalous Hall effect alongside a possible topological Hall signal confirms that the itinerant electrons are coupled to the ferromagnetism. Unlike the reported coexistence of FM and SC from two types of electrons, these observed significant properties of 2DEL are attributed solely to d_{xy} electrons. The observed coexistence of the FM and RSOC during the superconducting transition suggests a class of realistic platforms to investigate magnetization-controlled nonreciprocal transport properties near or inside the superconducting states. The combination of FM, RSOC, and SC at such oxide ferromagnet/superconductor heterointerfaces would offer a fascinating method to further investigate the nontrivial properties such as topological superconductivity, the spin-polarized supercurrents, and superconducting diode effect.

EXPERIMENTAL METHODS

Sample Fabrication

The 10 uc $LaAl_{0.7}Mn_{0.3}O_3$ thin films were epitaxially grown by pulsed laser deposition (PLD) using a KrF laser on TiO_2-terminated STO (001) substrates. A pulsed laser with a wavelength of 248 nm, a repetition frequency of 1 Hz, and a laser fluence of 2.0 J/cm^2 was used to ablate a $LaAl_{0.7}Mn_{0.3}O_3$ ceramic target. During the growth process, reflection high-energy electron diffraction (RHEED) was used to monitor in situ the film growth on unpatterned STO substrates. The first 4 uc buffer layer was deposited in 1×10^{-4} mbar of O_2 and then subsequently the last 6 uc top layer was grown in 1×10^{-5} mbar of O_2. The growth temperature was maintained at 650 °C, and the constant distance between target and substrate was ∼50 mm. After the growth of the film, the samples were cooled under deposition pressure at a rate of 10 °C/min to room temperature. Before the deposition, a hard mask made from amorphous $LaMnO_3$ (LMO) was patterned on the STO substrates in a Hall bar geometry by optical lithography for transport measurements.

STEM and EELS Analysis

The atomic-scale structural characterization of the 10 uc $LA_{0.7}M_{0.3}O_3$/STO heterostructure was conducted using a spherical aberration-corrected transmission electron microscope JEM NeoARM200 (JEOL, Ltd., Tokyo) operated at an accelerating voltage of 200 kV. Analysis of the STEM data and denoise processing were performed using the Gatan Digital Micrograph software.

Transport Characterization

The LI 5640 lock-in amplifiers with an AC excitation current of 1 nA and 13.7 Hz were used to characterize transport properties in the Hall Bar geometry with ultrasonically wire-bonded aluminum wires as electrodes. The width (W) and length (L) of the Hall bar were 50 and 500 μm, respectively.[32] A tunable DC bias current was provided by a Keithley 2401 source meter connected in series with a 10 MΩ resistor. A New Oxford Triton 200 dilution refrigerator system with a base temperature of 70 mK was used for measuring the transport properties with a perpendicular magnetic field (B).

Synchrotron Radiation Based Characterization

We performed XAS, XMCD, and XLD measurements at the Mn and Ti $L_{2,3}$ edges in total electron yield mode at the Deimos beamline, synchrotron Soleil.[71] The dichroic XMCD signal was recorded as the difference in the X-ray absorption spectra measured under a magnetic field of $B = \pm 6.5$ T applied perpendicular to the sample surface, with a parallel (σ^+)/antiparallel (σ^-) circular helicity beam. The XLD signal was recorded as the difference in the X-ray absorption spectra with horizontal (LH) and vertical (LV) linear polarized beam as σ_{LH}-σ_{LV}, and with the sample aligned at a grazing angle of 35 degree. Thus, the XAS from horizontal (LH) and vertical (LV) linear polarized X-beams, σ_{LH} and σ_{LV}, are sensitive to the $E//c$-axis and $E//ab$-plane, respectively.

ASSOCIATED CONTENT

Supporting Information

The Supporting Information is available free of charge at https://pubs.acs.org/doi/10.1021/acsnano.5c17832.

> The fabrication of ferromagnet/superconductor heterostructure ($LaAl_{0.7}Mn_{0.3}O_3/SrTiO_3$); X-ray diffraction characterization; analysis of the typical onset transition temperature; analysis of weak antilocalization; hysteretic magneto transport of H1; the synchrotron radiation based magnetic characterization; the transport characterizations of H2 (PDF)

AUTHOR INFORMATION

Corresponding Authors

Yulin Gan − *National Synchrotron Radiation Laboratory, School of Nuclear Science and Technology, University of Science and Technology of China, Hefei 230026, China;* orcid.org/0000-0003-0486-7026; Email: ylgan@ustc.edu.cn

Kai Chen − *National Synchrotron Radiation Laboratory, School of Nuclear Science and Technology, University of Science and Technology of China, Hefei 230026, China;* orcid.org/0000-0002-7667-3063; Email: kaichen2021@ustc.edu.cn

Hong Ding − *Tsung-Dao Lee Institute, Shanghai Jiao Tong University, Shanghai 200240, China; Beijing National Center for Condensed Matter Physics and Institute of Physics, Chinese Academy of Sciences, Beijing 100190, China;* Email: dingh@sjtu.edu.cn

Zhaoliang Liao − *National Synchrotron Radiation Laboratory, School of Nuclear Science and Technology, University of Science and Technology of China, Hefei 230026, China;* orcid.org/0000-0003-1701-9456; Email: zliao@ustc.edu.cn

Authors

Yuhao Hong − *National Synchrotron Radiation Laboratory, School of Nuclear Science and Technology, University of Science and Technology of China, Hefei 230026, China*

Guang Yang − *Beijing National Center for Condensed Matter Physics and Institute of Physics, Chinese Academy of Sciences, Beijing 100190, China*

Qinghua Zhang − *Beijing National Center for Condensed Matter Physics and Institute of Physics, Chinese Academy of Sciences, Beijing 100190, China*

Wen Xiao − *National Synchrotron Radiation Laboratory, School of Nuclear Science and Technology, University of Science and Technology of China, Hefei 230026, China*

Lei Wang − *National Synchrotron Radiation Laboratory, School of Nuclear Science and Technology, University of Science and Technology of China, Hefei 230026, China*

Shilin Hu − *National Synchrotron Radiation Laboratory, School of Nuclear Science and Technology, University of Science and Technology of China, Hefei 230026, China*

Jie Shen − *Beijing National Center for Condensed Matter Physics and Institute of Physics, Chinese Academy of Sciences, Beijing 100190, China;* orcid.org/0000-0002-7205-5081

Lei Yan − *Beijing National Center for Condensed Matter Physics and Institute of Physics, Chinese Academy of Sciences, Beijing 100190, China*

Li Lu − *Beijing National Center for Condensed Matter Physics and Institute of Physics, Chinese Academy of Sciences, Beijing 100190, China*

Philippe Ohresser − *Synchrotron SOLEIL, L'Orme des Merisiers, 91190 Saint Aubin, France*

Complete contact information is available at:
https://pubs.acs.org/10.1021/acsnano.5c17832

Notes

The authors declare no competing financial interest.

ACKNOWLEDGMENTS

The authors are thankful for the discussion with F. Yang. The work is supported by the fellowship of the National Key R&D Program of China (2022YFA1403000, 2024YFA1409500) and the National Natural Science Foundation of China (12275272, 12488101, 12204523); the Quantum Science and Technology−National Science and Technology Major Project (2021ZD0302700); the CAS Project for Young Scientists in Basic Research (YSBR-100); the China Postdoctoral Science Foundation (2020M680726, YJ20200325); and the Xiaomi Young Scholar Program. We acknowledge the synchrotron beamtime and user support from MCD-A and MCD-B (Soochow Beamline for Energy Materials) at NSRL, China and the Deimos beamline at Synchrotron Soleil.

REFERENCES

(1) Linder, J.; Robinson, J. W. A. Superconducting Spintronics. *Nat. Phys.* **2015**, *11* (4), 307−315.

(2) Trier, F.; Noël, P.; Kim, J.-V.; Attané, J.-P.; Vila, L.; Bibes, M. Oxide Spin-Orbitronics: Spin−Charge Interconversion and Topological Spin Textures. *Nat. Rev. Mater.* **2022**, *7* (4), 258−274.

(3) Lutchyn, R. M.; Bakkers, E. P. A. M.; Kouwenhoven, L. P.; Krogstrup, P.; Marcus, C. M.; Oreg, Y. Majorana Zero Modes in Superconductor-Semiconductor Heterostructures. *Nat. Rev. Mater.* **2018**, *3* (5), 52−68.

(4) Sau, J. D.; Lutchyn, R. M.; Tewari, S.; Das Sarma, S. Generic New Platform for Topological Quantum Computation Using Semiconductor Heterostructures. *Phys. Rev. Lett.* **2010**, *104* (4), No. 040502.

(5) Fu, L.; Kane, C. L. Superconducting Proximity Effect and Majorana Fermions at the Surface of a Topological Insulator. *Phys. Rev. Lett.* **2008**, *100* (9), No. 096407.

(6) Alicea, J. Majorana Fermions in a Tunable Semiconductor Device. *Phys. Rev. B* **2010**, *81* (12), No. 125318.

(7) Kezilebieke, S.; Huda, M. N.; Vano, V.; Aapro, M.; Ganguli, S. C.; Silveira, O. J.; Głodzik, S.; Foster, A. S.; Ojanen, T.; Liljeroth, P. Topological Superconductivity in a van Der Waals Heterostructure. *Nature* **2020**, *588* (7838), 424−428.

(8) Nadeem, M.; Fuhrer, M. S.; Wang, X. The Superconducting Diode Effect. *Nat. Rev. Phys.* **2023**, *5* (10), 558−577.

(9) Guo, L.; Yan, Y.; Xu, R.; Li, J.; Zeng, C. Zero-Bias Conductance Peaks Effectively Tuned by Gating-Controlled Rashba Spin-Orbit Coupling. *Phys. Rev. Lett.* **2021**, *126* (5), No. 057701.

(10) Jouan, A.; Singh, G.; Lesne, E.; Vaz, D. C.; Bibes, M.; Barthélémy, A.; Ulysse, C.; Stornaiuolo, D.; Salluzzo, M.; Hurand, S.; Lesueur, J.; Feuillet-Palma, C.; Bergeal, N. Quantized Conductance in a One-Dimensional Ballistic Oxide Nanodevice. *Nat. Electron.* **2020**, *3* (4), 201−206.

(11) Reyren, N.; Thiel, S.; Caviglia, A. D.; Kourkoutis, L. F.; Hammerl, G.; Richter, C.; Schneider, C. W.; Kopp, T.; Ruetschi, A.-S.; Jaccard, D.; Gabay, M.; Muller, D. A.; Triscone, J.-M.; Mannhart, J. Superconducting Interfaces between Insulating Oxides. *Science* **2007**, *317* (5842), 1196−1199.

(12) Caviglia, A. D.; Gariglio, S.; Reyren, N.; Jaccard, D.; Schneider, T.; Gabay, M.; Thiel, S.; Hammerl, G.; Mannhart, J.; Triscone, J. M. Electric Field Control of the $LaAlO_3/SrTiO_3$ Interface Ground State. *Nature* **2008**, *456* (7222), 624−627.

(13) Sun, Y.; Liu, Y.; Hong, S.; Chen, Z.; Zhang, M.; Xie, Y. Critical Thickness in Superconducting $LaAlO_3$/ $KTaO_3$(111) Heterostructures. *Phys. Rev. Lett.* **2021**, *127* (8), No. 086804.

(14) Chen, Z.; Liu, Z.; Sun, Y.; Chen, X.; Liu, Y.; Zhang, H.; Li, H.; Zhang, M.; Hong, S.; Ren, T.; Zhang, C.; Tian, H.; Zhou, Y.; Sun, J.; Xie, Y. Two-Dimensional Superconductivity at the $LaAlO_3/KTaO_3$ (110) Heterointerface. *Phys. Rev. Lett.* **2021**, *126* (2), No. 026802.

(15) Prawiroatmodjo, G. E. D. K.; Trier, F.; Christensen, D. V.; Chen, Y.; Pryds, N.; Jespersen, T. S. Evidence of Weak Superconductivity at the Room-Temperature Grown $LaAlO_3/SrTiO_3$ Interface. *Phys. Rev. B* **2016**, *93* (18), 184504.

(16) Brinkman, A.; Huijben, M.; Van Zalk, M.; Huijben, J.; Zeitler, U.; Maan, J. C.; Van Der Wiel, W. G.; Rijnders, G.; Blank, D. H. A.; Hilgenkamp, H. Magnetic Effects at the Interface between Non-Magnetic Oxides. *Nat. Mater.* **2007**, *6* (7), 493−496.

(17) Zhang, J.; Zhang, H. H.; Zhang, H. H.; Ma, Y.; Chen, X.; Meng, F.; Qi, S.; Chen, Y.; Hu, F.; Zhang, Q.; Liu, B.; Shen, B.; Zhao, W.; Han, W.; Sun, J. Long-Range Magnetic Order in Oxide Quantum Wells Hosting Two-Dimensional Electron Gases. *ACS Appl. Mater. Interfaces* **2020**, *12* (25), 28775−28782.

(18) Zhang, H.; Yun, Y.; Zhang, X.; Zhang, H.; Ma, Y.; Yan, X.; Wang, F.; Li, G.; Li, R.; Khan, T.; Chen, Y.; Liu, W.; Hu, F.; Liu, B.; Shen, B.; Han, W.; Sun, J. High-Mobility Spin-Polarized Two-Dimensional Electron Gases at $EuO/KTaO_3$ Interfaces. *Phys. Rev. Lett.* **2018**, *121* (11), No. 116803.

(19) Zhang, Y.; Gan, Y. L.; Zhang, H. R.; Zhang, H.; Norby, P.; Shen, B. G.; Sun, J. R.; Chen, Y. Z. Metallic Conduction and Ferromagnetism in $MAl_2O_4/SrTiO_3$ Spinel/Perovskite Heterostructures (M = Fe, Co, Ni). *Appl. Phys. Lett.* **2018**, *113* (26), No. 261603.

(20) Zhang, H.; Yan, X.; Zhang, H.; Wang, F.; Gu, Y.; Ning, X.; Khan, T.; Li, R.; Chen, Y.; Liu, W.; Wang, S.; Shen, B.; Sun, J. Magnetic Two-Dimensional Electron Gases with High Curie Temperatures at $LaAlO_3/SrTiO_3$:Fe Interfaces. *Phys. Rev. B* **2018**, *97* (15), 155150.

(21) Zhang, H. R.; Zhang, Y.; Zhang, H. R.; Zhang, J.; Shen, X.; Guan, X. X.; Chen, Y. S. Z.; Yu, R. C.; Pryds, N.; Chen, Y. S. Z.; Shen, B. G.; Sun, J. R. Magnetic Two-Dimensional Electron Gas at the Manganite-Buffered $LaAlO_3/SrTiO_3$ Interface. *Phys. Rev. B* **2017**, *96* (19), 195167.

(22) Caviglia, A. D.; Gabay, M.; Gariglio, S.; Reyren, N.; Cancellieri, C.; Triscone, J.-M. Tunable Rashba Spin-Orbit Interaction at Oxide Interfaces. *Phys. Rev. Lett.* **2010**, *104* (12), No. 126803.

(23) Wang, S.; Zhang, H.; Zhang, J.; Li, S.; Luo, D.; Wang, J.; Jin, K.; Sun, J. Circular Photogalvanic Effect in Oxide Two-Dimensional Electron Gases. *Phys. Rev. Lett.* **2022**, *128* (18), No. 187401.

(24) Xu, H.; Li, H.; Gauquelin, N.; Chen, X.; Wu, W.; Zhao, Y.; Si, L.; Tian, D.; Li, L.; Gan, Y.; Qi, S.; Li, M.; Hu, F.; Sun, J.; Jannis, D.; Yu, P.; Chen, G.; Zhong, Z.; Radovic, M.; Verbeeck, J.; Chen, Y.; Shen, B. Giant Tunability of Rashba Splitting at Cation-Exchanged Polar Oxide Interfaces by Selective Orbital Hybridization. *Adv. Mater.* **2024**, *36* (29), No. 2313297.

(25) Zhang, H.; Yan, X.; Zhang, X.; Wang, S.; Xiong, C.; Zhang, H.; Qi, S.; Zhang, J.; Han, F.; Wu, N.; Liu, B.; Chen, Y.; Shen, B.; Sun, J. Unusual Electric and Optical Tuning of $KTaO_3$ -Based Two-Dimensional Electron Gases with 5d Orbitals. *ACS Nano* **2019**, *13* (1), 609−615.

(26) Huang, J.; Cheng, L.; Li, J.; Lin, T.; Zhou, T.; Chen, J.; Zhao, Y.; Li, M.; Shi, W.; Zhang, Q.; Su, J.; Chen, Y. A Two-Dimensional Electron Gas at the Sulfurized $SrTiO_3$ Interface. *J. Phys. Chem. C* **2025**, *129* (42), 19118−19123.

(27) Chen, Z.; Liu, Y.; Zhang, H.; Liu, Z.; Tian, H.; Sun, Y.; Zhang, M.; Zhou, Y.; Sun, J.; Xie, Y. Electric Field Control of Superconductivity at the $LaAlO_3/KTaO_3$ (111) Interface. *Science* **2021**, *372* (6543), 721−724.

(28) Gan, Y.; Yang, F.; Kong, L.; Chen, X.; Xu, H.; Zhao, J.; Li, G.; Zhao, Y.; Yan, L.; Zhong, Z.; Chen, Y.; Ding, H. Light-Induced Giant Rashba Spin−Orbit Coupling at Superconducting $KTaO_3(110)$ Heterointerfaces. *Adv. Mater.* **2023**, *35* (25), No. 2300582.

(29) Herranz, G.; Singh, G.; Bergeal, N.; Jouan, A.; Lesueur, J.; Gázquez, J.; Varela, M.; Scigaj, M.; Dix, N.; Sánchez, F.; Fontcuberta, J. Engineering Two-Dimensional Superconductivity and Rashba Spin−Orbit Coupling in $LaAlO_3/SrTiO_3$ Quantum Wells by Selective Orbital Occupancy. *Nat. Commun.* **2015**, *6* (1), 6028.

(30) Stornaiuolo, D.; Cantoni, C.; De Luca, G. M.; Di Capua, R.; Di Gennaro, E.; Ghiringhelli, G.; Jouault, B.; Marre, D.; Massarotti, D.; Miletto Granozio, F.; Pallecchi, I.; Piamonteze, C.; Rusponi, S.; Tafuri, F.; Salluzzo, M. Tunable Spin Polarization and Superconductivity in Engineered Oxide Interfaces. *Nat. Mater.* **2016**, *15* (3), 278−283.

(31) Fix, T.; MacManus-Driscoll, J. L.; Blamire, M. G. Delta-Doped $LaAlO_3/SrTiO_3$ Interfaces. *Appl. Phys. Lett.* **2009**, *94* (17), No. 172101.

(32) Gan, Y.; Christensen, D. V.; Zhang, Y.; Zhang, H.; Krishnan, D.; Zhong, Z.; Niu, W.; Carrad, D. J.; Norrman, K.; von Soosten, M.; Jespersen, T. S.; Shen, B.; Gauquelin, N.; Verbeeck, J.; Sun, J.; Pryds, N.; Chen, Y. Diluted Oxide Interfaces with Tunable Ground States. *Adv. Mater.* **2019**, *31* (10), No. 1805970.

(33) Mao, Z.; Qiu, D.; Xu, Z.; Hao, B.; Zhang, H.-Y.; Sun, H.; Pei, X.; Wang, M.; Li, Y.; Gu, Z.-B.; Zhu, Y.; Cheng, G.; Nie, Y. A Two-Dimensional Superconducting Electron Gas at $LaFeO_3$ /$SrTiO_3$ Interfaces. *Nano Lett.* **2025**, *25* (1), 586−592.

(34) Stornaiuolo, D.; Jouault, B.; Di Gennaro, E.; Sambri, A.; D'Antuono, M.; Massarotti, D.; Granozio, F. M.; Di Capua, R.; De Luca, G. M.; Pepe, G. P.; Tafuri, F.; Salluzzo, M. Interplay between Spin-Orbit Coupling and Ferromagnetism in Magnetotransport Properties of a Spin-Polarized Oxide Two-Dimensional Electron System. *Phys. Rev. B* **2018**, *98* (7), No. 075409.

(35) Zhang, H.; Xiao, Y.; Gao, Q.; Wu, N.; Zhou, S.; Wang, Y.; Wang, M.; Tian, D.; Chen, L.; Qi, W.; Zheng, D.; Zhang, J.; Han, F.; Yang, H.; Liu, B.; Chen, Y.; Hu, F.; Shen, B.; Sun, J.; Zhao, W.; Zhang, J. Magnetotransport Evidence for the Coexistence of Two-Dimensional Superconductivity and Ferromagnetism at (111)-Oriented a-$CaZrO_3/KTaO_3$ Interfaces. *Nat. Commun.* **2025**, *16* (1), 3035.

(36) Hua, X.; Zeng, Z.; Meng, F.; Yao, H.; Huang, Z.; Long, X.; Li, Z.; Wang, Y.; Wang, Z.; Wu, T.; Weng, Z.; Wang, Y.; Liu, Z.; Xiang, Z.; Chen, X. Superconducting Stripes Induced by Ferromagnetic Proximity in an Oxide Heterostructure. *Nat. Phys.* **2024**, *20*, 957−963.

(37) Zhao, Y.-C.; Li, J.-J.; Wang, Z.; Zhou, T.-L.; Li, M.-H.; Shi, W.-X.; Hu, F.-X.; Sun, J.-R.; Li, G.; Chen, Y.-Z.; Shen, B.-G. Spin-Polarized Two-Dimensional Electron Gas with Giant Rashba Splitting at the EuTiO3/$KTaO_3(111)$ Interface under Light Illumination. *Chin. Phys. Lett.* **2025**, *42* (10), No. 100703.

(38) Gan, Y.; Zhang, Y.; Christensen, D. V.; Pryds, N.; Chen, Y. Gate-Tunable Rashba Spin-Orbit Coupling and Spin Polarization at Diluted Oxide Interfaces. *Phys. Rev. B* **2019**, *100* (12), No. 125134.

(39) Niu, W.; Liu, W.; Gu, M.; Chen, Y. Y. Y.; Zhang, X.; Zhang, M.; Chen, Y. Y. Y.; Wang, J.; Du, J.; Song, F.; Pan, X.; Pryds, N.; Wang, X.; Wang, P.; Xu, Y.; Chen, Y. Y. Y.; Zhang, R. Direct Demonstration of the Emergent Magnetism Resulting from the Multivalence Mn in a $LaMnO_3$ Epitaxial Thin Film System. *Adv. Electron. Mater.* **2018**, *4* (6), No. 1800055.

(40) Chen, Y. Z.; Trier, F.; Wijnands, T.; Green, R. J.; Gauquelin, N.; Egoavil, R.; Christensen, D. V.; Koster, G.; Huijben, M.; Bovet, N.; Macke, S.; He, F.; Sutarto, R.; Andersen, N. H.; Sulpizio, J. A.; Honig, M.; Prawiroatmodjo, G. E. D. K.; Jespersen, T. S.; Linderoth, S.; Ilani, S.; Verbeeck, J.; Van Tendeloo, G.; Rijnders, G.; Sawatzky, G. A.; Pryds, N. Extreme Mobility Enhancement of Two-Dimensional Electron Gases at Oxide Interfaces by Charge-Transfer-Induced Modulation Doping. *Nat. Mater.* **2015**, *14* (8), 801−806.

(41) Chen, Y. Z.; Döbeli, M.; Pomjakushina, E.; Gan, Y. L.; Pryds, N.; Lippert, T. Scavenging of Oxygen Vacancies at Modulation-Doped Oxide Interfaces: Evidence from Oxygen Isotope Tracing. *Phys. Rev. Mater.* **2017**, *1* (5), No. 052002.

(42) Ahadi, K.; Galletti, L.; Li, Y.; Salmani-Rezaie, S.; Wu, W.; Stemmer, S. Enhancing Superconductivity in SrTiO3 Films with Strain. *Sci. Adv.* **2019**, *5* (4), n/a.

(43) Pai, Y.-Y.; Lee, H.; Lee, J.-W.; Annadi, A.; Cheng, G.; Lu, S.; Tomczyk, M.; Huang, M.; Eom, C.-B.; Irvin, P.; Levy, J. One-Dimensional Nature of Superconductivity at the $LaAlO_3/SrTiO_3$ Interface. *Phys. Rev. Lett.* **2018**, *120* (14), No. 147001.

(44) Dikin, D. A.; Mehta, M.; Bark, C. W.; Folkman, C. M.; Eom, C. B.; Chandrasekhar, V. Coexistence of Superconductivity and Ferromagnetism in Two Dimensions. *Phys. Rev. Lett.* **2011**, *107* (5), No. 56802.

(45) Maekawa, S.; Fukuyama, H. Magnetoresistance in Two-Dimensional Disordered Systems: Effects of Zeeman Splitting and Spin-Orbit Scattering. *J. Phys. Soc. Jpn.* **1981**, *50* (8), 2516−2524.

(46) Gunkel, F.; Bell, C.; Inoue, H.; Kim, B.; Swartz, A. G.; Merz, T. A.; Hikita, Y.; Harashima, S.; Sato, H. K.; Minohara, M.; Hoffmann-Eifert, S.; Dittmann, R.; Hwang, H. Y. Defect Control of Conventional and Anomalous Electron Transport at Complex Oxide Interfaces. *Phys. Rev. X* **2016**, *6* (3), No. 031035.

(47) Li, M. H.; Li, H.; Gan, Y. L.; Xu, H.; Xiong, C. M.; Hu, F. X.; Sun, J. R.; Schmitt, T.; Strocov, V. N.; Chen, Y. Z.; Shen, B. G. Decoupling the Conduction from Redox Reaction and Electronic Reconstruction at Polar Oxide Interfaces. *Phys. Rev. Mater.* **2022**, *6* (3), No. 35004.

(48) Li, H.; Gan, Y.; Husanu, M.-A.; Dahm, R. T.; Christensen, D. V.; Radovic, M.; Sun, J.; Shi, M.; Shen, B.; Pryds, N.; Chen, Y. Robust Electronic Structure of Manganite-Buffered Oxide Interfaces with Extreme Mobility Enhancement. *ACS Nano* **2022**, *16* (4), 6437−6443.

(49) Joshua, A.; Pecker, S.; Ruhman, J.; Altman, E.; Ilani, S. A Universal Critical Density Underlying the Physics of Electrons at the $LaAlO_3/SrTiO_3$ Interface. *Nat. Commun.* **2012**, *3* (1), 1129.

(50) Nagaosa, N.; Sinova, J.; Onoda, S.; MacDonald, A. H.; Ong, N. P. Anomalous Hall Effect. *Rev. Mod. Phys.* **2010**, *82* (2), 1539−1592.

(51) Wang, W.; Daniels, M. W.; Liao, Z.; Zhao, Y.; Wang, J.; Koster, G.; Rijnders, G.; Chang, C.-Z. Z.; Xiao, D.; Wu, W. Spin Chirality Fluctuation in Two-Dimensional Ferromagnets with Perpendicular Magnetic Anisotropy. *Nat. Mater.* **2019**, *18* (10), 1054−1059.

(52) Liu, J.; Zhang, X.; Ji, Y.; Gao, X.; Wu, J.; Zhang, M.; Li, L.; Liu, X.; Yan, W.; Yao, T.; Yin, Y.; Wang, L.; Guo, H.; Cheng, G.; Wang, Z.; Gao, P.; Wang, Y.; Chen, K.; Liao, Z. Controllable Itinerant Ferromagnetism in Weakly Correlated 5d SrIrO $_3$. *J. Phys. Chem. Lett.* **2022**, *13* (51), 11946−11954.

(53) Shin, H.; Liu, C.; Godin, S.; Li, F.; Sutarto, R.; Davidson, B. A.; Zou, K. Highly Tunable Ferromagnetic 2D Electron Gases at Oxide Interfaces. *Adv. Mater. Interfaces* **2022**, *9* (32), No. 2201475.

(54) Zhong, X.; Oubla, M.; Wang, X.; Huang, Y.; Zeng, H.; Wang, S.; Liu, K.; Zhou, J.; He, L.; Zhong, H.; Alonso-Vante, N.; Wang, C.-W.; Wu, W.-B.; Lin, H.-J.; Chen, C.-T.; Hu, Z.; Huang, Y.; Ma, J. Boosting Oxygen Reduction Activity and Enhancing Stability through Structural Transformation of Layered Lithium Manganese Oxide. *Nat. Commun.* **2021**, *12* (1), 3136.

(55) Lee, J. S.; Xie, Y. W.; Sato, H. K.; Bell, C.; Hikita, Y.; Hwang, H. Y.; Kao, C. C. Titanium d_{xy} Ferromagnetism at the $LaAlO_3/SrTiO_3$ Interface. *Nat. Mater.* **2013**, *12* (8), 703−706.

(56) Salluzzo, M.; Gariglio, S.; Torrelles, X.; Ristic, Z.; Di Capua, R.; Drnec, J.; Sala, M. M.; Ghiringhelli, G.; Felici, R.; Brookes, N. B. Structural and Electronic Reconstructions at the $LaAlO_3$/ $SrTiO_3$ Interface. *Adv. Mater.* **2013**, *25* (16), 2333−2338.

(57) Cao, Y.; Liu, X.; Shafer, P.; Middey, S.; Meyers, D.; Kareev, M.; Zhong, Z.; Kim, J. W.; Ryan, P. J.; Arenholz, E.; Chakhalian, J. Anomalous Orbital Structure in a Spinel-Perovskite Interface. *npj Quantum Mater.* **2016**, *1*, n/a.

(58) Mocuta, C.; Ohresser, P.; Barbier, A. Artificial Laminar Oxide Multiferroic Magnetoelectric Thin Film Structures - Elaboration Methods and Study by Synchrotron Radiation Techniques. *OAJ. Mater. Devices* **2022**, *5* (2), n/a.

(59) Thole, B. T.; Carra, P.; Sette, F.; Van Der Laan, G. X-Ray Circular Dichroism as a Probe of Orbital Magnetization. *Phys. Rev. Lett.* **1992**, *68* (12), 1943−1946.

(60) Chen, C. T.; Idzerda, Y. U.; Lin, H.-J.; Smith, N. V.; Meigs, G.; Chaban, E.; Ho, G. H.; Pellegrin, E.; Sette, F. Experimental Confirmation of the X-Ray Magnetic Circular Dichroism Sum Rules for Iron and Cobalt. *Phys. Rev. Lett.* **1995**, *75* (1), 152−155.

(61) Mehta, M. M.; Dikin, D. A.; Bark, C. W.; Ryu, S.; Folkman, C. M.; Eom, C. B.; Chandrasekhar, V. Evidence for Charge−Vortex Duality at the LaAlO3/SrTiO3 Interface. *Nat. Commun.* **2012**, *3* (1), 955.

(62) Yadav, S.; Kaushik, V.; Saravanan, M. P.; Sahoo, S. Probing Electron-Electron Interaction along with Superconducting Fluctuations in Disordered TiN Thin Films. *Phys. Rev. B* **2023**, *107* (1), No. 014511.

(63) Lopes Dos Santos, J. M. B.; Abrahams, E. Superconducting Fluctuation Conductivity in a Magnetic Field in Two Dimensions. *Phys. Rev. B* **1985**, *31* (1), 172−176.

(64) Larkin, A. I. Reluctance of Two-Dimensional Systems. *J. Exp. Theor. Phys. Lett.* **1980**, *31* (4), 239−243.

(65) Chen, Z.; Wang, B. Y.; Swartz, A. G.; Yoon, H.; Hikita, Y.; Raghu, S.; Hwang, H. Y. Universal Behavior of the Bosonic Metallic Ground State in a Two-Dimensional Superconductor. *Npj Quantum Mater.* **2021**, *6* (1), 15.

(66) Moetakef, P.; Williams, J. R.; Ouellette, D. G.; Kajdos, A. P.; Goldhaber-Gordon, D.; Allen, S. J.; Stemmer, S. Carrier-Controlled Ferromagnetism in $SrTiO_3$. *Phys. Rev. X* **2012**, *2* (2), 039901.

(67) Li, B.; Roschewsky, N.; Assaf, B. A.; Eich, M.; Epstein-Martin, M.; Heiman, D.; Münzenberg, M.; Moodera, J. S. Superconducting Spin Switch with Infinite Magnetoresistance Induced by an Internal Exchange Field. *Phys. Rev. Lett.* **2013**, *110* (9), No. 097001.

(68) Yi, H.; Hu, L.-H.; Wang, Y.; Xiao, R.; Cai, J.; Hickey, D. R.; Dong, C.; Zhao, Y.-F.; Zhou, L.-J.; Zhang, R.; Richardella, A. R.; Alem, N.; Robinson, J. A.; Chan, M. H. W.; Xu, X.; Samarth, N.; Liu, C.-X.; Chang, C.-Z. Crossover from Ising- to Rashba-Type Superconductivity in Epitaxial Bi_2Se_3/Monolayer $NbSe_2$ Heterostructures. *Nat. Mater.* **2022**, *21* (12), 1366−1372.

(69) Yoshizawa, S.; Kobayashi, T.; Nakata, Y.; Yaji, K.; Yokota, K.; Komori, F.; Shin, S.; Sakamoto, K.; Uchihashi, T. Atomic-Layer Rashba-Type Superconductor Protected by Dynamic Spin-Momentum Locking. *Nat. Commun.* **2021**, *12* (1), 1462.

(70) He, J. J.; Tanaka, Y.; Nagaosa, N. The Supercurrent Diode Effect and Nonreciprocal Paraconductivity Due to the Chiral Structure of Nanotubes. *Nat. Commun.* **2023**, *14* (1), 3330.

(71) Ohresser, P.; Otero, E.; Choueikani, F.; Chen, K.; Stanescu, S.; Deschamps, F.; Moreno, T.; Polack, F.; Lagarde, B.; Daguerre, J.-P.; Marteau, F.; Scheurer, F.; Joly, L.; Kappler, J.-P.; Muller, B.; Bunau, O.; Sainctavit, Ph DEIMOS: A Beamline Dedicated to Dichroism Measurements in the 350−2500 eV Energy Range. *Rev. Sci. Instrum.* **2014**, *85* (1), No. 013106.